Tissue-based Biomarker Investigation Guided by Functional Immuno-oncology Platform in Ovarian Cancer

Master's Programme in Translational Medicine and Study Track Cancer
Master's thesis

Author:
Aditi Sirsikar

Supervisor(s):
MD, PhD Anniina Färkkilä
PhD Ashwini Sakrepatna Nagaraj

29.4.2024
Helsinki

Abstract:

Ovarian cancer remains a significant health challenge worldwide, with high-grade serous carcinoma (HGSC) representing its most aggressive subtype. Despite advancements in treatment, disease recurrence remains high, with most patients relapsing within a few years, necessitating the investigation of novel and combination therapies. This study presents a robust framework for evaluating the efficacy of immuno-oncology agents in HGSC through the establishment of a high-throughput patient-derived immunocompetent culture (iPDC) drug screening platform. Using an in-house analysis pipeline to harmonize the complex data outputted by our high-throughput model, we found significant reductions in live tumor cell abundance in response to ataxia telangiectasia and Rad3-related inhibitor (ATRi) in targeting tumor cells irrespective of homologous recombination (HR) status. However, certain samples exhibit immune cell toxicity, emphasizing the importance of assessing immune cell-specific responses for comprehensive evaluation of therapy outcomes. The tissue-based investigation further validates these findings, revealing elevated DNA damage and replication stress biomarker, pRPA32-RPA2(Ser8), expression in responders to ATRi combinations, corroborating previous research and suggesting promising therapeutic targets. Moreover, analysis of immune cell abundance and functional states underscores the predominance of myeloid cells in the tumor microenvironment (TME), with limited variation observed in T-cell activation between responders and non-responders to ATRi. Spatial analysis reveals distinct intertumoral immune infiltration patterns, potentially influencing treatment responses. Overall, these results shed light on the intricate interplay between tumor biology and therapeutic response in HGSC, offering insights into tailored treatment strategies and emphasizing the need for personalized approaches in oncology.

Keywords: High-grade ovarian carcinoma, Patient-derived immunocompetent cultures, Precision oncology, ATR inhibitors (ATRi), tCycIF

Table of contents

1 Literature Review

1.1 High-grade serous ovarian cancer

1.1.1 Epidemiology and clinical characteristics of HGSC

Ovarian cancer is the leading cause of mortality among gynecologic malignancies, posing a significant burden on women's health globally (Momenimovahed et al., 2019). In 2023, the National Cancer Institute estimated 19,710 women will be diagnosed with ovarian cancer and 67% of patients will die from this disease in the United States (Siegel et al., 2023). Likewise, in Finland, roughly 60% of women diagnosed with ovarian cancer succumb to their disease (Finnish Cancer Registry, 2023).

High-grade serous carcinoma (HGSC) is the most common and aggressive subtype of ovarian cancer and accounts for 70-80% of all ovarian cancer deaths (Bowtell et al., 2015). Arising from secretory epithelial cells of the distal fallopian tube and surface epithelial cells of the ovary, HGSC often eludes early detection, manifesting predominantly in advanced stages (III, IV). In many cases, treatment is started after the malignancy has disseminated into adjacent pelvic organs, the omentum, and extraperitoneal regions (Lisio et al., 2019).

1.1.2 Standard primary treatment

Standard treatment begins with primary debulking surgery (PDS) followed by platinum- and taxane-based chemotherapy. Removing all cancerous tissue is rarely achievable, especially in advanced stages of disease, necessitating chemotherapy following macroscopic tumor debulking surgery. Standard postoperative intravenous chemotherapy consists of six cycles of intravenous carboplatin/paclitaxel combination therapy administered every three weeks (Armstrong et al., 2021).

Platinum and taxane compounds induce apoptosis by interfering with cell replication and cell growth. Carboplatin forms lesions on purine bases of DNA inducing G2/M growth arrest and eventually cell death (Rabik & Dolan, 2007). Mechanistically, paclitaxel stabilizes microtubules against depolymerization required during chromosomal segregation resulting in M growth arrest and apoptosis-inducing factor release from mitochondria (Mikuła-Pietrasik et al., 2019). At the University of Helsinki Hospital, most patients receive an angiogenesis inhibitor, bevacizumab, during

primary treatment in addition to chemotherapy. Bevacizumab has been shown to improve progression-free survival in advanced ovarian cancer cases, however demonstrating modest improvement in overall survival (Matulonis et al., 2016). Despite minimal residual disease following cytoreductive surgery and complete response to first-line therapy (no evidence of disease on CT imaging and normal CA - 125 levels), 70% of patients relapse within three years of initial treatment (Ledermann et al., 2012).

1.2 Advancements in maintenance therapy for HGSC

1.2.1 Targeted monotherapies and combination strategies

Recent and ongoing clinical trials have examined the safety and efficacy of targeted monotherapies and combination therapies such as Poly (ADP-ribose) polymerase (PARP) inhibitors (Coleman et al., 2019; González-Martín et al., 2019; Moore et al. 2018; Ray-Coquard et al., 2019), angiogenesis inhibitors (Ray-Coquard et al., 2019), and immune checkpoint inhibitors (Konstantinopoulos et al., 2019) to prevent the progression or recurrence of HGSC. Additionally, the efficacy of immuno-oncology combination therapies has shown promising results in acquired platinum-resistant and platinum-refractory ovarian cancer. Findings from the Topacio phase I/II trial demonstrated synergistic effects of niraparib, a PARP inhibitor, and pembrolizumab, an immune checkpoint inhibitor, exceeding the efficacy of these therapies as monotherapies (Konstantinopoulos et al., 2019).

1.2.2 Considerations in maintenance therapy selection

Decisions about which maintenance therapy to administer depend on several factors including mutation status, pathologic stage of disease, primary systemic therapy, response to primary therapy, and the patient's overall health (Armstrong et al., 2021). PARP inhibitors, such as olaparib and niraparib, target DNA repair mechanisms and are particularly effective against platinum-sensitive tumor cells characterized by genomic instability or homologous recombination repair deficiency (HRD)(Ledermann et al., 2012). Bevacizumab is a monoclonal antibody that neutralizes vascular endothelial growth factor-A, a protein responsible for facilitating tumor angiogenesis. Bevacizumab monotherapy is recommended to patients, at high risk for disease progression, who are not good candidates for PARP inhibitors (Oza et

al., 2015; Ray-Coquard et al., 2019). Immune checkpoint inhibitors such as pembrolizumab act as an anti-programmed cell death protein 1 (PD-1) antibody enhancing T-cell activity against tumor cells. However, the efficacy of anti-PD-1 antibodies is predicated upon PD ligand 1 (PD-L1) expression and the prevalence of tumor-infiltrating lymphocytes (TILs) within the tumor microenvironment (Bogani et al., 2020). While the armament of targeted therapies is expanding, the challenge remains in identifying which patients are likely to benefit from each targeted therapy.

1.3 Patient stratification by tumor molecular profile

1.3.1 Genomic characteristics of HGSC

TP53 mutations are ubiquitous in HGSC and are present in nearly all patients. Other notable features include somatic copy number alterations, somatic point variants, and DNA homologous recombination repair deficiency (HRD), primarily attributed to germline and somatic variants of *BRCA1/2* (The Cancer Genome Atlas Research Network, 2011). BRCA1/2 are responsible for repairing DNA damage, necessary to maintain genomic stability, and promote cell survival.

Chromosomal instability and HRD affect 50% of HGSC cases, leading to the accumulation of copy number alterations and potentially promoting adaptive tumor responses (Li & Heyer, 2008). Amplification and increased expression of *CCNE1* contribute to aberrant DNA replication, centrosome amplification, and chromosomal instability (Chan et al., 2020). *CCNE1* amplification is observed in up to one-fifth of HGSCs and is linked to resistance against platinum agents, PARP inhibitors, and poor prognosis (Lheureux et al., 2020).

1.3.2 Targeted therapies for subset of HGSC patients

In patients with defective HR DNA repair, PARP inhibitors have shown remarkable success clinically as a maintenance therapy (Figure 1) extending progression-free survival (Moore et al., 2018; Ray-Coquard et al., 2019) and demonstrating clinically meaningful improvement in overall survival (DiSilvestro et al., 2023). PARP inhibitors amplify DNA damage and cancer cell death by preventing the repair of single-strand DNA breaks and inducing double-strand DNA breaks in cells already hampered by genomic instability; thereby selectively inducing synthetic lethality in cancer cells (Rose et al., 2020). Efforts to improve the detection of homologous recombination have

enhanced patient selection for HR-targeted therapy (Perez-Villatoro et al., 2022). However, PARP inhibitors are not suitable for a sizable proportion of HGSC cases. Additional investigation of targeted therapies for patients with homologous recombination proficiency (HRP), platinum resistance, and acquired PARP inhibitor resistance is required.

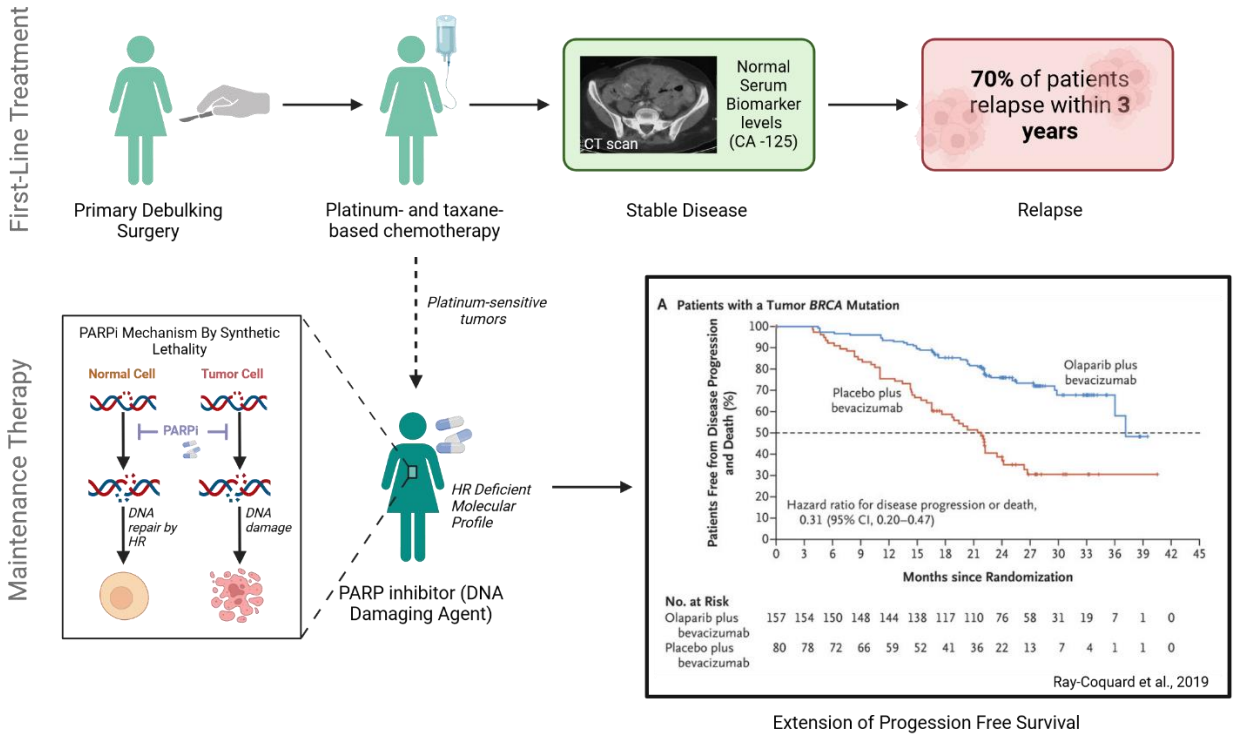

Figure 1. Standard treatment for patients with homologous recombination deficiency. Schematic depicting standard first-line and maintenance treatments for patients with platinum-sensitive tumors and HRD molecular profile. Findings from the phase 3 PAOLA-1 trial demonstrate the efficacy of PARP inhibitor, olaparib, as a maintenance treatment for patients with a germline *BRCA* mutation. The Kaplan-Meyer plot, Figure 3A of Ray-Coquard et al., 2019, shows the median progression-free survival in the olaparib group was 37.2 months versus 21.7 months in the placebo group. Created with BioRender.com

1.4 The role of the TME in tumorigenesis and immunotherapy development

1.4.1 Tumor microenvironment in ovarian cancer

The tumor microenvironment (TME) in ovarian cancer is characterized by peritoneal metastasis and the generation of malignant ascites. Metastatic spread involves direct shedding into the ascites and migration throughout the peritoneal cavity, often resulting in tumor deposits on omental tissue, a fatty layer covering the surface of

abdominal organs. Within the microenvironment, interactions among tumor cells, stromal cells, and myeloid and lymphoid immune cells, have been shown to regulate tumor progression (Ning et al., 2021).

1.4.2 Immunosuppressive and immunocompetent components of the TME

Myeloid cells, integral components of the innate immune system, influence the tumor microenvironment by initiating inflammatory responses such as engulfing apoptotic tumor cells and facilitating antigen presentation. Conversely, myeloid cells also contribute to tissue remodeling and tumor progression (Kloosterman & Akkari, 2023). Macrophages represent a significant portion of myeloid cells present in the TME of HGSCs (Launonen et al., 2022). Tumor-associated macrophages (TAMs) emerge as key regulators in ovarian TME, suppressing anti-tumor immune responses by impeding the functions of cytotoxic T-cells while promoting regulatory T-cells (Curiel et al., 2004; Lecker et al., 2021). Accumulating evidence indicates that high infiltration of TAMs correlates with poor prognosis in ovarian cancer (Hensler et al., 2020; Larionova et al., 2020).

Furthermore, anti-tumor immune cells, such as CD3+ tumor-infiltrating lymphocytes (TILs), play a critical role in recognizing tumor neoantigens and inducing tumor cell apoptosis. TILs can be further divided into CD4+ helper T-cells and CD8+ cytotoxic T-cells, both of which are associated with increased survival (Hao et al., 2020).

1.4.3 Immunotherapy challenges and opportunities in HGSC

Despite evidence of immunogenicity in high-grade ovarian cancer, immune checkpoint inhibitors (ICI) targeting PD-1/L1 in combination with standard adjuvant chemotherapy provide no significant benefit (Moore et al., 2021). Ongoing research into cell dynamics and spatial interactions within the tumor microenvironment holds promise for identifying patients who may benefit from specific immunotherapy strategies.

For instance, a spatial tissue-based investigation revealed distinct tumor microenvironments characterized by enhanced spatial immunosurveillance, particularly in *BRCA1/2*-mutant tumors (Launonen et al., 2022). Higher proportions of CD8+ and CD4+ T-cells were linked to improved prognosis. Additionally, in *BRCA1/2*-mutated tumors, the proximity of CD8+ and CD4+ T-cells to proliferating

epithelial cells was associated with extended platinum-free intervals, regardless of cell abundances. Further investigations leveraging the dynamic interplay between tumor and immune cells are warranted to address drug resistance and immune escape mechanisms. Moreover, these discoveries motivate preclinical studies examining the potential synergistic effects of immuno-oncology therapies, which could offer long-term benefits.

1.4.4 Modeling tumor microenvironment in patient-derived cultures

Advanced modeling techniques and innovative co-culture systems have deepened our understanding of the tumor immune microenvironment and its response to immunotherapies. For instance, researchers have successfully propagated patient-derived organoids while preserving native tumor epithelia along with embedded immune cells, including tumor-infiltrating lymphocytes (Neal et al., 2018). Furthermore, a novel HGSC organoid/immune cell co-culture platform, treated with bispecific anti-PD-1/PD-L1 antibodies, revealed key targets for immune checkpoint blockade therapy, such as natural killer cells and specific T-cell subsets, previously overlooked by monospecific treatments (Wan et al., 2021). Most notably, researchers could predict clinical response to PD-1 blockade by assessing immune cell reactivation capacity, and they identified tumor-resident T-cells as pivotal for the immunological response (Voabil et al., 2021).

Although patient-derived *ex vivo* models offer valuable insights into the TME and provide platforms for refining immunotherapy strategies in cancer treatment, their reliance on murine tissue-derived matrigel or collagen-based matrices for culturing cells and tissue poses limitations in modeling human TME. Moreover, previous research focusing on patient-derived models has primarily concentrated on assessing the effects of immune checkpoint inhibitors on immune cell functionality, neglecting to consider the cytotoxic effect on tumor cells. Additionally, most of these models have not demonstrated scalability to accommodate high-throughput combinatorial drug testing.

2 Introduction

2.1 Background

To study the effect of novel single agents and immuno-oncology combination therapies across different molecular subtypes of HGSC, our lab developed a high-throughput screening platform using HGSC patient-derived immunocompetent cultures (iPDCs) grown in a tumor-free patient-derived omentum gel matrix (OmeGel), while preserving native tumor-infiltrating immune cells. The omentum, predominantly composed of adipocytes, is the primary site of metastasis for HGSC and has been shown to promote rapid tumor growth both in *in vitro* and *in vivo* models (Nieman et al., 2011).

We validated that OmeGel, as reported by Neilson et al. (2023), significantly enhances the growth of patient-derived HGSC samples compared to an animal-derived basement membrane matrix. Furthermore, the iPDCs recapitulated HRD-specific responses to PARP inhibitors, and iPDCs derived from chemotherapy and PARPi refractory tumors mirrored clinical outcomes (Nagaraj et al., 2024). Next, my colleagues established eight patient-derived iPDCs in a 384-well format to perform high-throughput drug testing of single agents and combination treatments including DNA damaging agents: PARP inhibitors (PARPi), ATR inhibitors (ATRi), WEE1 inhibitors (WEE1i), an established immunotherapy agent, Pembrolizumab (anti-PD-1), and novels immunotherapies such as ATX inhibitor (ATXi) and PERK inhibitor (PERKi) (Table 1).

Table 1. List of single agents tested in iPDCs.

Drug	Category	Rationale
Olaparib (PARPi)	DNA damaging agent	PARPi is effective in HGSC patients with HRD (Ray-Coquard et al., 2019)
AZD6379 (ATRi)	DNA damaging agent	Cell cycle checkpoint inhibitor, ataxia telangiectasia and Rad3-related inhibitor (ATRi), is effective in HGSC with elevated replication stress (Li et al., 2022)
Adavosertib (WEE1i)	DNA damaging agent	Cell cycle checkpoint inhibitor, WEE1i, exacerbates DNA replication stress and showed clinical efficacy in combination with gemcitabine in HGSC (Lheureux et al., 2021)

Pembrolizumab (anti-PD-1)	Immunotherapy	Immune checkpoint inhibitor, anti-PD-1, enhances T-cell activity against tumor cells and shows promising anti-tumor activity in combination with niraparib in HGSC patients (Konstantinopoulos et al., 2019)
GLPG1690 (ATXi)	Novel immunotherapy	Genetic ablation of the LPA-generating enzyme autotaxin (ATX) has been shown to activate infiltrating lymphocytes by inducing interferon signaling in dendritic cells (Chae et al., 2022)
AMG PERK 44 (PERKi)	Novel Immunotherapy	Deletion of PKR-like endoplasmic reticulum kinase (PERK) reprogrammed tumor-associated myeloid-derived suppressor cells into immunocompetent myeloid cells (Mohamed et al., 2020)

To measure drug response, immunofluorescence staining and high-content imaging were used to determine single-cell cytotoxic responses from tumor and immune cells. High-content single-cell image acquisition was performed using the Opera Phenix High-Content Screening System. In total, 60 mono- and combination-treatments were tested per sample. Each treatment combination was dispensed in four wells. Between ten to fifteen images were taken per well. For every patient, approximately 40-60 images were taken per treatment condition. The cells in each well were stained for CK7 (for tumor cells), CD45 (for immune cells), DAPI (nuclear DNA marker), and dead cell marker (Figure 2).

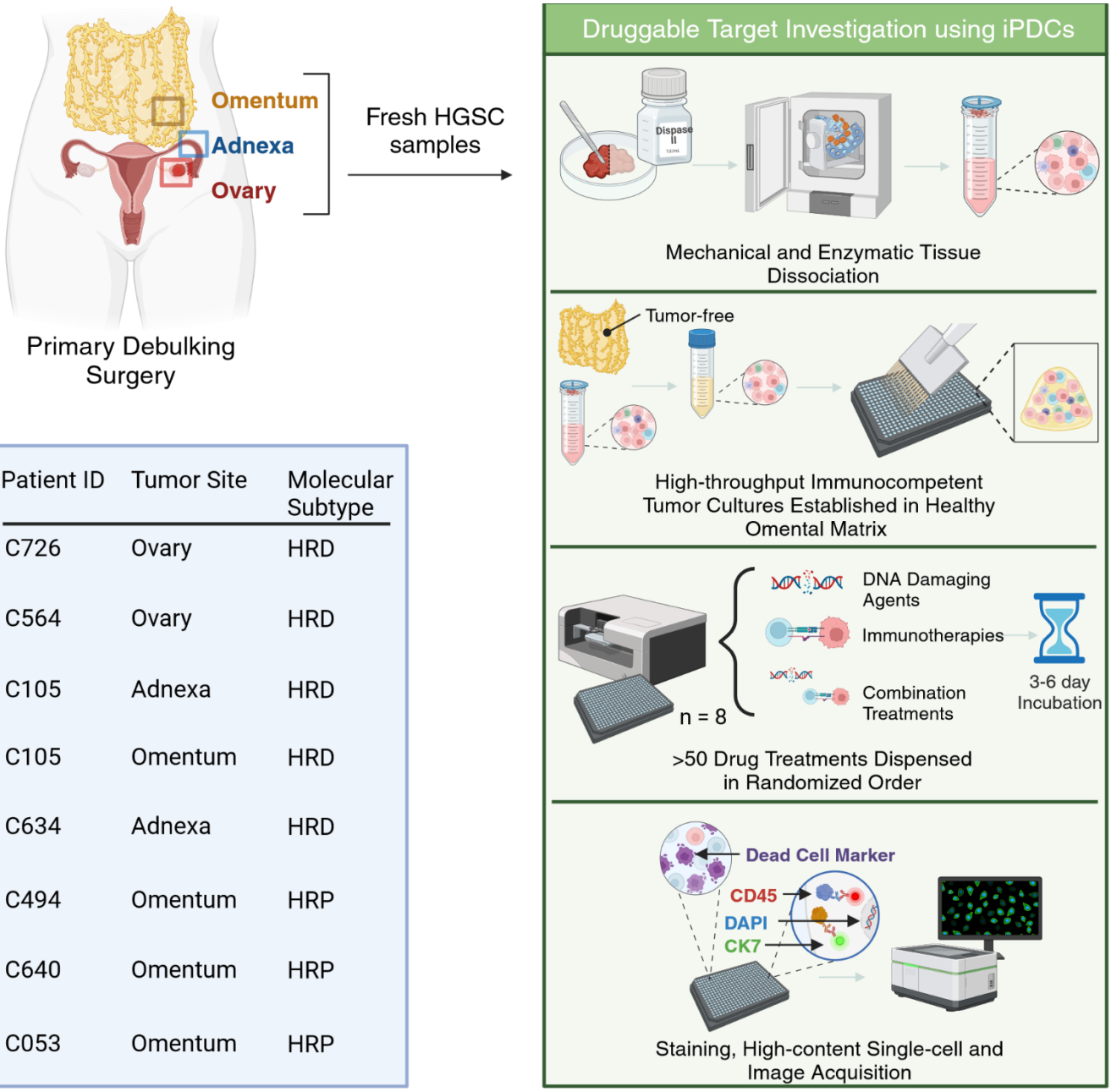

Patient ID	Tumor Site	Molecular Subtype
C726	Ovary	HRD
C564	Ovary	HRD
C105	Adnexa	HRD
C105	Omentum	HRD
C634	Adnexa	HRD
C494	Omentum	HRP
C640	Omentum	HRP
C053	Omentum	HRP

Figure 2. Schematic of iPDC establishment and drug screening protocol. Briefly, fresh samples resected during the primary debulking surgery were mechanically and chemically dissociated into a single cell suspension. Dissociated tumor cells are added to tumor-free patient-derived omentum matrix (Omegel), blood clotting factors like aprotinin, thrombin, and fibrinogen were added to solidify the Omegel, and the resulting suspension was rapidly plated in a 384-well plate. The following day, therapeutic agents including DNA damaging drugs and immunotherapies were dispensed in a randomized fashion by the Digital Dispenser (Tecan D300e). Following 3-6 days of incubation, the cells were stained with dead cell marker, fixed, and then stained with anti-CD45, DAPI, and anti-CK7 antibodies. Using the Opera Phenix High-Content Screening System, 10-15 images were taken per well. iPDCs for eight patients were established; the patient sample information is summarized in a table on the left. Created with BioRender.com

2.2 Aims

Researchers in our lab established the iPDCs and performed high-throughput drug testing and high-content imaging; however, we had no methods to analyze this complex data. The first aim of my thesis was to develop a data analysis pipeline to systematically process, analyze, and visually represent our results.

Next, I used tissue cyclic multiplex immunofluorescence (tCycIF) on corresponding formalin-fixed paraffin-embedded (FFPE) tumor tissues obtained from the same samples cultured in the iPDCs to validate the results produced by the drug screening platform. Guided by the findings in the iPDCs, I aimed to compare the load of replication stress in tumor cells from samples that responded and did not respond to ATRi using downstream targets phosphorylation of checkpoint kinase 1 (pCHK1) and replication stress protein A (RPA32/ RPA2(Ser8)), which are validated predictive biomarkers of ATRi sensitivity (Bradbury et al., 2022). In addition, immune cell markers and functional immune markers were included in the experimental panel to comment on immune cell abundance, functional states, and spatial characteristics within the TME. This tissue-based biomarker investigation guided by a functional immuno-oncology platform aimed to demonstrate the utility of this entire platform in testing potential combination therapies to elucidate patient-specific differences within the TME that influence drug sensitivity.

3 Materials and Methods

3.1 Materials

3.1.1 Samples

In accordance with the ethical standard from the 1975 Declaration of Helsinki and approved by the Ethics Committee of the Women's Clinic, the Helsinki University Hospital, and the Helsinki Biobank, patient samples and clinical data used in the following experiments were obtained from consenting participants of the ONCOSYS-OVA study (clinical trial number: NCT06117384). One portion of the fresh tissue obtained from the primary debulking surgery was processed in the iPDCs, while another portion of the same tissue was formalin-fixed and paraffin-embedded. Sample collection and processing were performed by colleagues in the lab.

3.1.2 Reagents and Instruments

Table 2. Compilation of reagent and instruments.

Reagent/ Instrument	Catalog number	Manufacturer
Absolute Ethanol	13210132	Berner
Xylene, ACS, 99%	10741624	AcrosOrganics
10X PBS (Diluted 1:10)	10649743	Fisher
Hydrogen peroxide 30%	BP2633500/10386643	Fisher
Citric acid Monohydrate	C1909-2.5KG	Sigma
Sodium Hydroxide	1064621000	Sigma
Odyssey blocking buffer	927-40150	Li-COR
Glycerol	G5516	Sigma
Glass microscope slides (75x25 mm)	631-9483	ThermoScientific
Cover glass (24x60 mm)	15356429/235503601	Fisher
Beurer TL30 Lamp	418715	Beurer
CyteFinder II		Rarecyte

3.1.3 Antibody panel

Table 3. Summary of antibodies.

Antibody (Cycle)	Fluoro-chrome	Comp-any	Cat number	Clone	Concen-tration	Target
DAPI (1)	361	Invitrogen	H3570	*blank*	10000	Nucleus
pCHK1 (1)	unconj (488)	CST	2348S	133D3	50	pCHK1
Granzyme B (1)	unconj (647)	Dako	M7235	GrB-7	50	Activated cytotoxic T and NK cells
CD68 (2)	488	CST	24850S	D4B9C	100	Myeloid
Phospho-Stat1 (Y701) (2)	555	CST	8183S	58D6	100	Activated INF-y pathway + cytotoxic T and NK cells
CD8a (2)	660	Invitrogen	50-0008-80	AMC908	150	Cytotoxic T-cells
Vimentin (2)	750	CST	9855S	D21H3	100	Stromal cell marker
Phospho-RPA32/RPA2(Ser8) (3)	488	CST	31912S	E5A2F	100	RPA32/ RPA2(Ser8)
CD3D (3)	555	Abcam	ab208514	EP4426	100	T cells
PD1 (3)	647	Abcam	ab201825	EPR4877(2)	150	T cell exhaustion
CD4 (4)	488	RnD systems	FAB8165G	*blank*	150	Helper T-cells
CD11C (4)	555	CST	77882BC	D3V1E	150	Dendritic cells
Pax8 (5)	488	Abcam	ab214955	EPR18715	150	HGSC (carcinoma)
FoxP3 (5)	555	Invitrogen	41-4777-80	236A/E7	100	Regulatory T-cells
HLA-DPB1 (5)	647	Abcam	ab201347	EPR11226	400	MHC II
CK7 (6)	555	Abcam	ab209601	EPR17078	200	Tumor
gH2Ax (6)	647	BioLegend	613407	2F3	150	DNA Damage

3.2 Methods

3.2.1 tCycIF protocol

3.2.1.1 Sample sectioning, dewaxing, antigen retrieval, and pre-staining

FFPE tissue sections, 4µm thick, were prepared by the histopathology services at FIMM. The tCycIF protocol begins with baking the slides in the oven at 56 °C for 30 minutes to ensure tissue adherence to the microscopic slide, followed by dewaxing and rehydration. The slides soaked in cuvettes containing xylene for 5 minutes, three times. To ensure complete dehydration, the slides were immersed for three minutes in serial alcohol solutions (100% ethanol, 90% ethanol, 70% ethanol, 50% ethanol, 30% ethanol) followed by two washed in 1x PBS for one minute each. To initiate antigen retrieval, the slides were immersed in a glass dish containing 250ml of a 10M citric acid solution with a pH of 6 and heated in the microwave. The slides rested at room temperature for 20 minutes. Following this, they underwent a 30-minute incubation with Odyssey blocking buffer at room temperature. Subsequent steps involved pre-staining the slides with DAPI and secondary antibodies for an hour at room temperature, followed by three washes in 1x PBS. Lastly, fluorophores conjugated to the secondary antibodies were inactivated by bleaching the slides and rinsing them four times with 1x PBS.

3.2.1.2 Antibody Staining

The antibody panel (Table 3) includes antibodies required to phenotype tumor, immune, and stromal cells, in addition to functional tumor and immune markers. Following pre-staining, the first cycle of unconjugated primary antibodies were incubated overnight at 4°C. DAPI, Alexa-488, and -647 secondary antibodies were added the next day and incubated at room temperature for an hour, followed by image acquisition. The antibodies in the following cycles were all conjugated primary antibodies and incubated overnight at 4°C.

3.2.1.3 Image Acquisition

Stained slides were scanned using the CyteFinder II, located in our lab. Per cycle, a maximum of five antibodies were scanned in one of the following channels: 361nm, 488nm, 555nm, 647nm, and 750nm. DAPI staining was constant throughout all six

cycles to register images from each cycle into one composite image per tissue section. Prior to scanning, the exposure time of the channel laser and Z axis of the slide stage were adjusted. A RCPNL file was outputted for each cycle scanned.

3.2.1.4 Bleaching/flourophore inactivation

After the pre-staining step and between each cycle, the fluorophores were inactivated in a solution of 40ml of 1x PBS, 7.5ml of 30% H2O2, and 2.5mL of 480 mM NaOH. The slides were submerged in this solution with LED lamps positioned directly above the plastic container with the slides and bleaching solution. The slides are bleached at room temperature for 90 minutes total. Following the pre-staining, the solution was refreshed after 30 mins and in the subsequent cycles was replaced after 45 minutes.

3.2.2 tCycIF image processing

Eight patient samples from post-debulking surgery were processed to obtain formalin-fixed paraffin-embedded (FFPE) tumor tissue sections. These sections underwent sequential staining with validated antibodies and were scanned using the RareCyte CyteFinder II system, following the t-CycIF protocol (Lin et al., 2018). Utilizing the ASHLAR algorithm (Muhlich et al., 2022), images from each staining cycle were stitched and registered to generate a single high-plex image. Nuclear segmentation was performed using the StarDist method, which identifies nuclei based on positive DAPI staining (Schmidt et al., 2018). Mean fluorescence intensity for all markers within each cell mask was quantified using a custom Python script. Any artifacts such as antibody aggregates, bubbles, signal over-exposure, and segmentation errors were addressed using CyLinter (Baker et al., 2023).

Manual gating was performed for each antibody per sample in Napari (Sofroniew et al., 2022), a multi-dimensional image viewer to visualize multiple markers at once and SCIMAP (Schapiro et al., 2022), a single-cell analysis toolkit. Next, in SCIMAP, cell type calling followed the logic tree summarized in Figure 3. The Mann-Whitney U test was performed to probe for between group differences in the proportions of functional marker in tumor and immune cells.

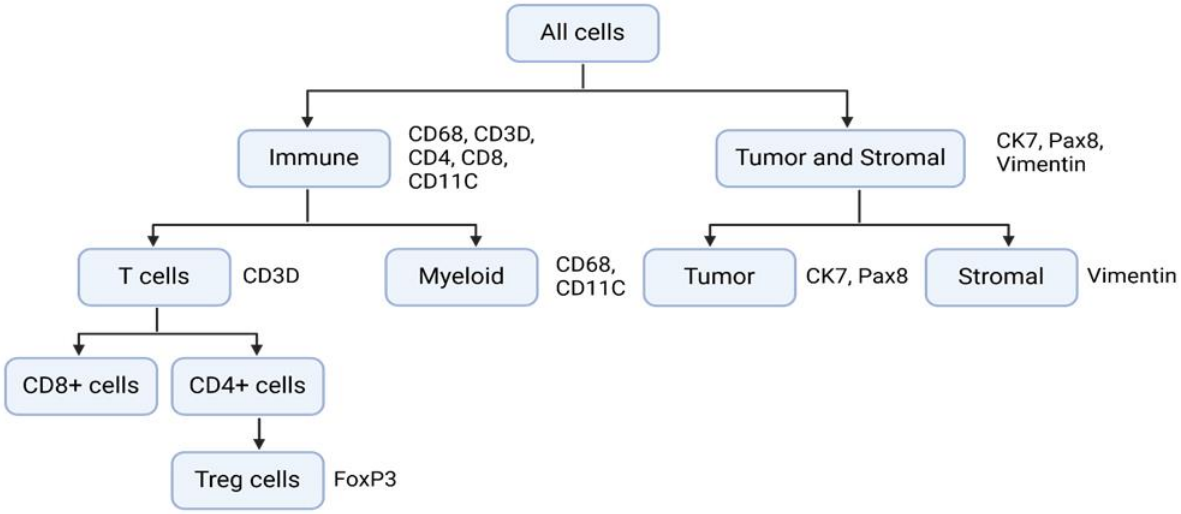

Figure 3. Phenotype logic tree. To assign cell types, this logic was used to perform cell phenotyping in SCIMAP. Created with BioRender.com

4 Results

4.1 Establishment of iPDC drug screening data analysis pipeline

4.1.1 Data analysis pipeline development

To harmonize the high-throughput quantified image data from iPDCs established for eight patients and comparatively visualize tumor and immune cell-specific responses following treatment with 60 different drug combinations in a 384-well layout, I developed a data processing pipeline in Rstudio, summarized by the panels within the black box in Figure 4. The pipeline integrates single-cell mean marker intensity values obtained from CellProfiler per sample, sample-specific marker thresholds, and a randomized drug dispenser layout to identify the treatment and concentration administered in each well per sample. This data is fed into the pipeline for multiple samples at once and visualized in a single heatmap. Developing the pipeline required revisiting the raw images to confirm the most accurate representation of the image data.

To account for inter-patient variability in *in vitro* cell growth, images containing no CK7+ cells, no CD45+ cells, and fewer than five cells total were removed. Images that had a total cell abundance greater than three standard deviations above the mean compared to other images from the same treatment were also filtered out. My colleague revisited the raw images and gated each marker, dead cell marker (DCM), CD45 (immune cell marker), and CK7 (cancer cell marker), per sample to accurately delineate between positive and negative cells. The pipeline labeled some cells as both CK7+ and CD45+, which is not biologically plausible. By revisiting the images, we determined that these cells were dead and more prone to form aggregates of non-specific markers. Therefore, any cell double-positive for tumor and immune markers was excluded from further analysis.

Given the varied cell proliferation rate between patient samples, the proportion of CK7+ alive over all alive cells per image, to quantify live tumor cell abundance, and CD45+ alive cells over all CD45+ cells, to quantify live immune cell abundance, were plotted. Immune cells made up a smaller fraction of the total cells across all samples; therefore, calculating the proportion of live CD45+ cells over the total number of CD45+ cells reduced bias introduced by varied total cell abundance across samples.

Reduced live tumor cell abundance reflects drug sensitivity and reduced live immune cell abundance reflects drug toxicity towards healthy off-target cells. To compare treatment sensitivity and toxicity across samples, the Wilcoxon signed-rank test was used to evaluate whether the change in live tumor and immune cell abundance per treatment significantly differed from the control (DMSO-treated) per sample.

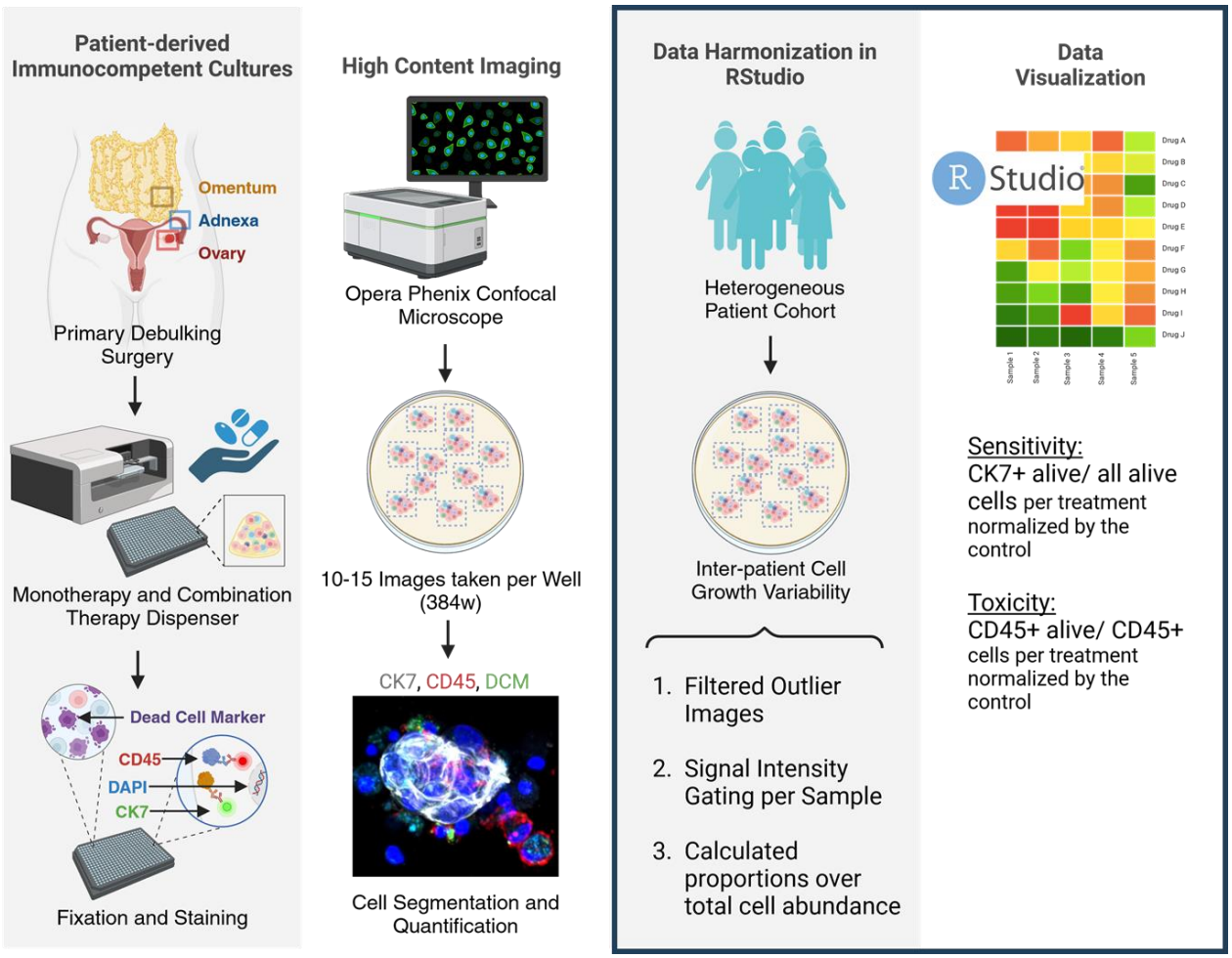

Figure 4. Development of data analysis pipeline. The third and fourth panel, highlighted by the black box, describe the data harmonization method and visualization of tumor and immune cell-specific responses to immuno-oncology mono- and combination treatments. Created with BioRender.com

4.1.2 Evaluation of iPDC sensitivity to immune-oncology therapy combinations

To comparatively visualize the analysis pipeline output, the Log2 fold change (Log2FC) of live tumor cell abundance ratios per treatment was normalized by the control and plotted (Figure 5). Unsupervised hierarchical clustering of live tumor cell abundance showed that samples clustered based on treatment response. Samples

C494, C053, C726, and C634 responded to single agent ATRi or ATRi in combination with another DNA damaging agent or immunotherapy, suggesting ATRi contributed to the reduction of live CK7+ cells compared to the control.

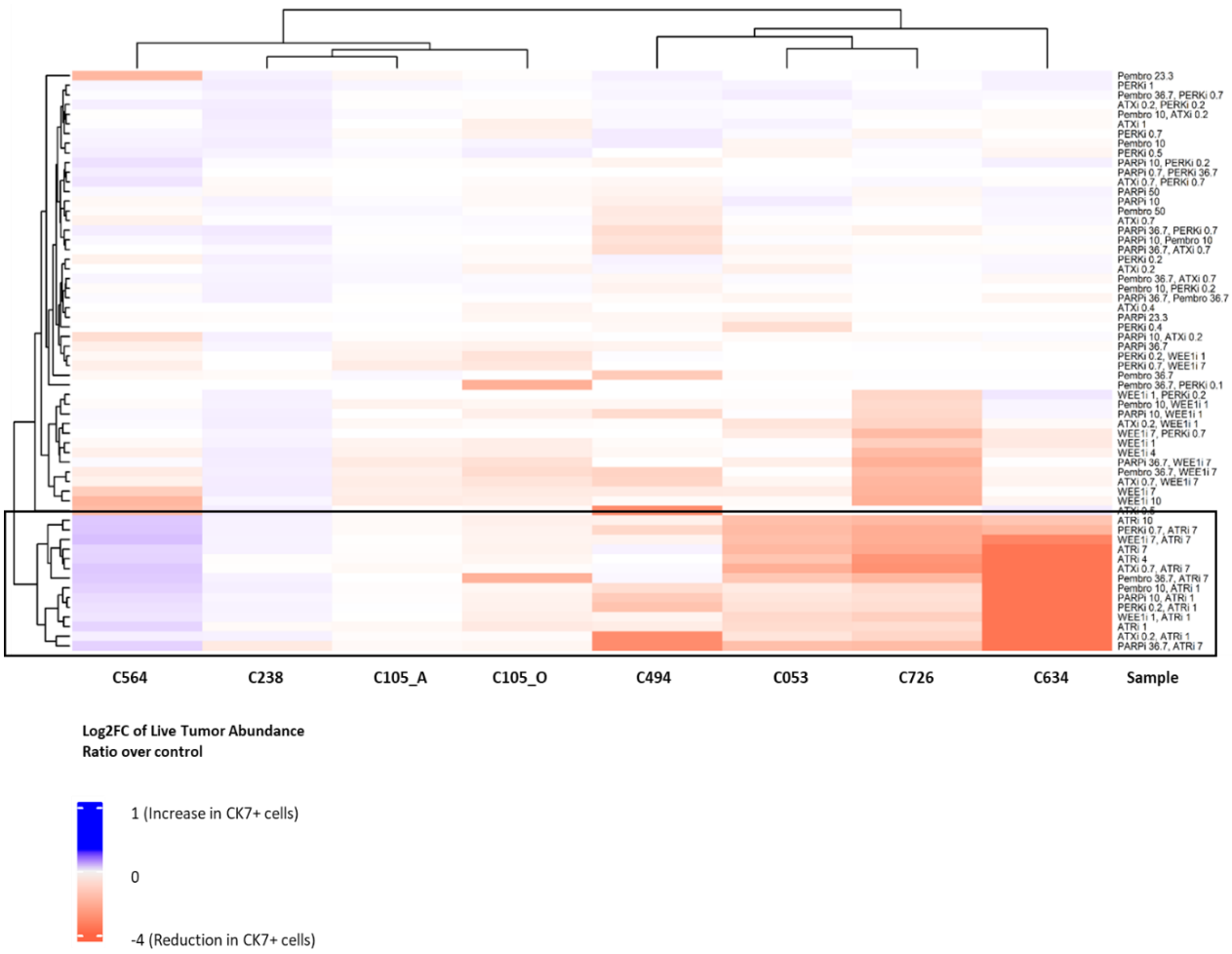

Figure 5. An unsupervised hierarchical clustered heatmap showing the Log2FC in live CK7+ tumor cells over all live cells in each treatment condition normalized by the control. The samples clustered based on drug response. The black box highlights the positive response in half of the patient samples to DNA damaging agent, ATRi, as a monotherapy or ATRi in combination with other agents.

4.1.3 Tumor and immune cell-specific responses to ATRi and combinations

Incorporating statistical findings about treatment efficacy show ATRi monotherapy and in combination significantly contributed to tumor cell death in a subset of samples (Figure 6). This effect was observed independent of tumor HR status. The analysis of CD45+ immune viability revealed patient-specific trends. In samples C053 and C634, ATRi single and combination treatments significantly reduced live CK7+ tumor cells in addition to significantly decreasing live CD45+ immune cells, suggesting the treatment

was toxic towards immune cells. However, in two responding iPDCs (C494 and C726), immune cell viability showed no significant change, suggesting the anti-tumor effects of ATRi and its combinations was greater than the immune cell toxicity. Conversely, in response to ATRi combinations, live CK7+ cell abundance increased while the abundance of live CD45+ immune cells decreased in samples C564 and C238. These findings demonstrate the efficacy of combining ATR inhibitors with DNA damaging agents like PARP inhibitors or WEE1 inhibitors, as well as immunotherapies such as anti-PD-1, ATX inhibitors, or PERK inhibitors against a subset of HGSC iPDCs. Crucially, this study emphasizes the importance of evaluating immune cell-specific death responses alongside tumor cell-specific responses to accurately assess the benefits of immuno-oncology combinations.

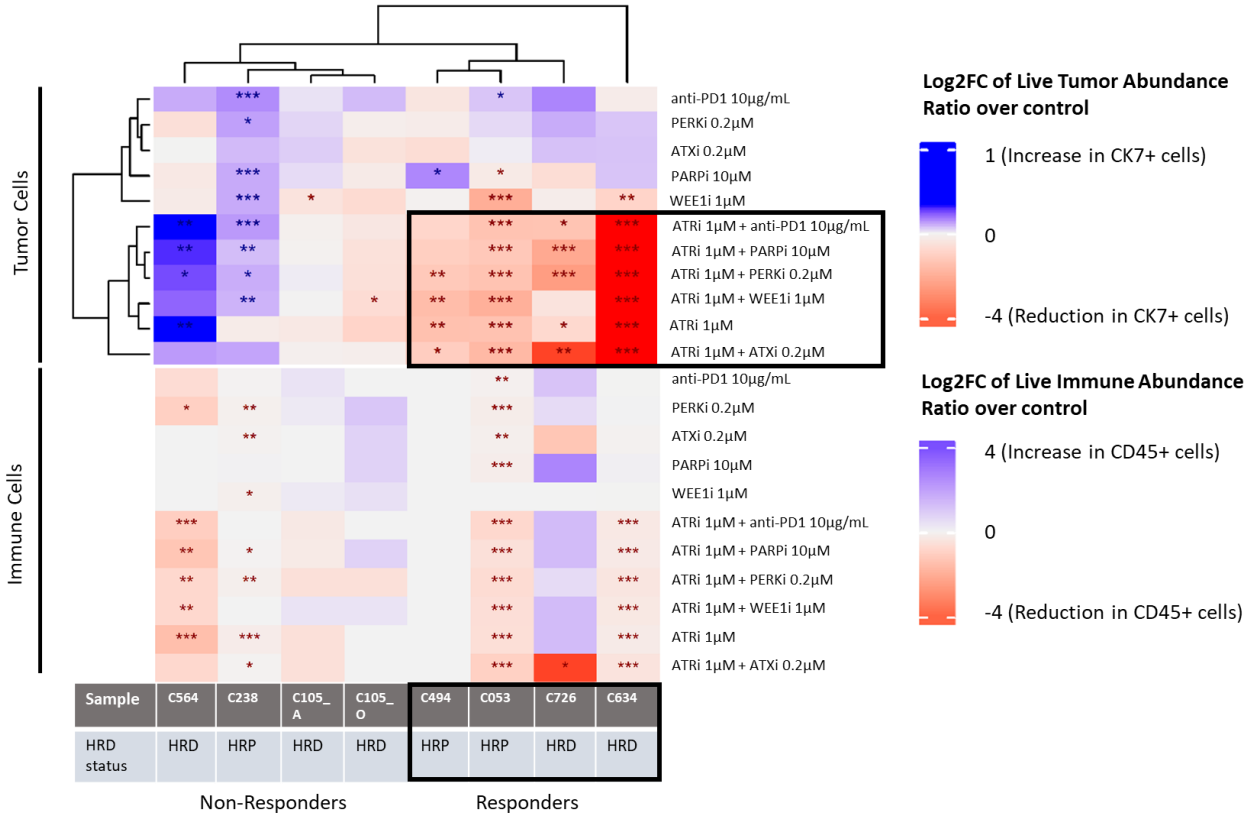

Figure 6. Patient-specific tumor and immune cell responses to ATRi and combinations. An unsupervised hierarchical clustering depicts the Log2FC in live CK7+ tumor cells relative to all live cells across each treatment condition, normalized to the control (top). The bottom heatmap illustrates the Log2FC in live CK45+ immune cells compared to all CD45+ cells within each treatment condition, normalized to the control. Wilcoxon signed rank test $p^* < 0.05$, $p^{**} < 0.01$, $p^{***} < 0.001$.

4.2 Tissue-based investigation of DNA damage and replication stress in responders and non-responders to ATRi combination treatments

4.2.1 Elevated DNA damage biomarker expression in responders

Gamma-H2AX (γH2AX) serves as a biomarker for genomic instability and double-strand DNA breaks, displaying heightened expression levels in ovarian tumor tissue compared to normal epithelial cells (Palla et al., 2017). Tumors burdened with DNA damage may exhibit increased susceptibility to exogenous DNA damaging agents. To investigate this hypothesis, we conducted tissue cyclic multiplex immunofluorescence (tCycIF) on corresponding formalin-fixed paraffin-embedded (FFPE) tumor tissues obtained from the samples depicted in Figure 6. This entailed using antibodies against PAX8 and CK7 (for tumor cells), vimentin (for stromal cells), and the DNA damage marker γH2AX. Single-cell analysis of tCycIF images targeting PAX8- or CK7-positive cancer cells expressing γH2AX revealed that tumor cells from samples sensitive to ATR inhibitor (ATRi), a DNA damaging agent, exhibited heightened DNA damage compared to non-responders (Figure 7). This result validates previous findings suggesting that elevated DNA damage serves as a predictor for sensitivity to ATRi and

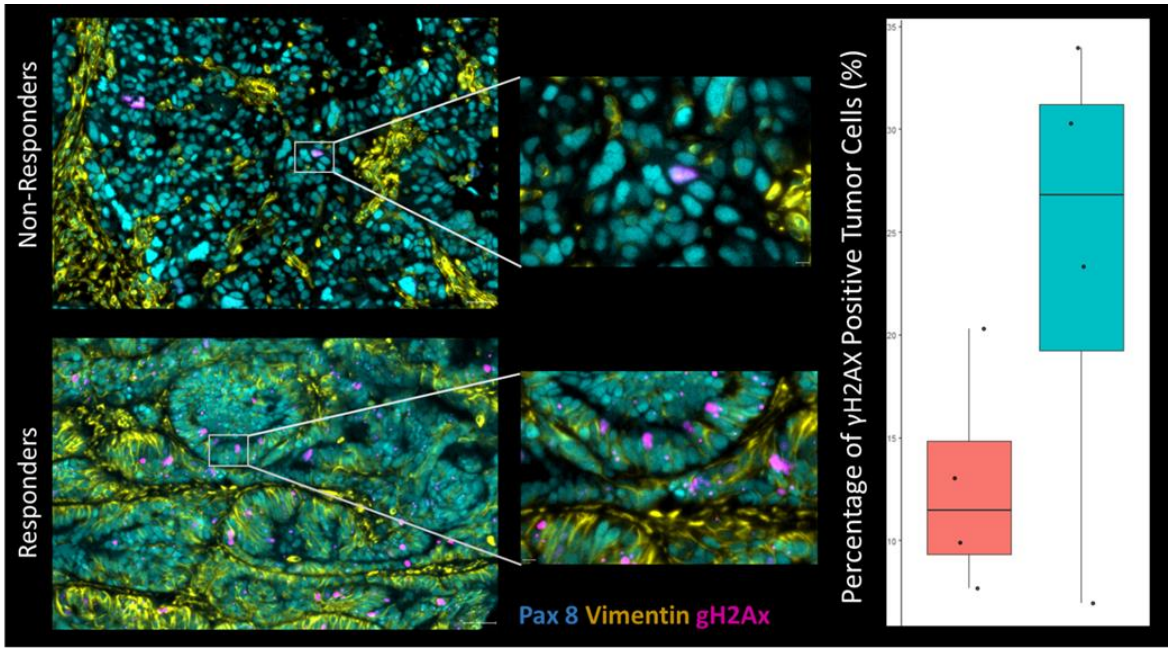

Figure 7. Elevated DNA damage in tumor cells of responders compared to non-responders. Box-and-whisker plot of tumor cells expressing γH2AX plotted as a percentage (right). Representative images from C105_A, non-responder, and C634, responder (left). Scale bar 150µm and 50µm.

its combinations (Bradbury et al., 2022). While these findings do not reach statistical significance, the observed trend is noteworthy.

4.2.2 Elevated replication stress biomarker expression in responders

An increase in replication stress marker, phosphorylated checkpoint kinase 1 (pCHK1), has been identified as a predictive biomarker for ATR inhibitor (ATRi) sensitivity (Bradbury et al., 2022). To assess if this correlation is also observed in our samples, we used antibodies against PAX8 and CK7 (for tumor cells), vimentin (for stromal cells), and the replication stress marker pCHK1. Single-cell analysis of tCycIF images for PAX8- or CK7-positive cancer cells expressing pCHK1 revealed that samples responsive to ATRi combinations exhibited elevated pCHK1 levels compared to non-responders (Figure 8). This result is limited by sample size and non-canonical antibody staining pattern. This anti-pCHK1 marker is a well characterized nuclear marker; however, cytoplasmic staining observed in a number of samples, seen in the close up representative image for responders (center bottom) in Figure 8, introduces potential technical or biological queries. These results suggest future testing with other antibodies specifically targeting nuclear pCHK1.

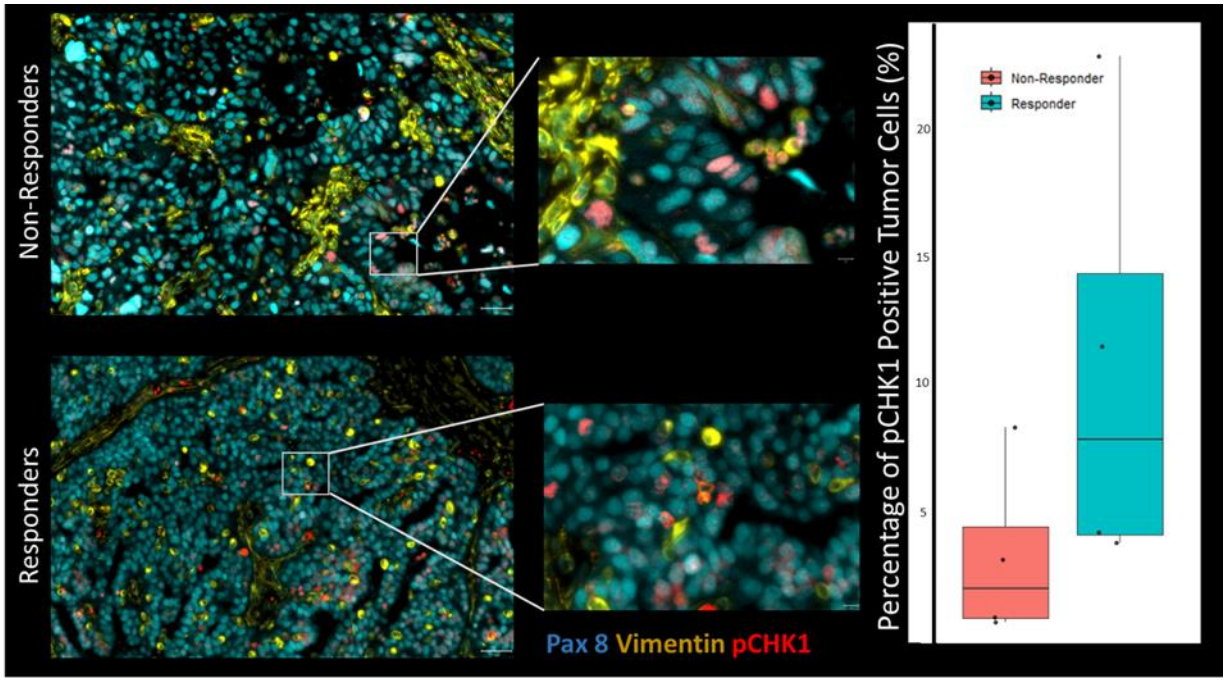

Figure 8. Elevated replication stress marker, pCHK1, in tumor cells of responders compared to non-responders. Box-and-whisker plot of tumor cells expressing pCHK1 plotted as a percentage (right). Representative images from C105_A, non-responder, and C634, responder (left). Scale bar 150μm and 50μm.

4.2.3 Significantly elevated downstream ATR target activation in responders versus non-responders

An increase in the replication stress marker, phosphorylated replication stress protein A (pRPA), a downstream target of pCHK1, has been identified as a predictive biomarker for ATRi sensitivity (Bradbury et al., 2022). To evaluate if this correlation holds true in our samples, we utilized antibodies against PAX8 and CK7 (for tumor cells), vimentin (for stromal cells), and the replication stress marker pRPA32-RPA2(Ser8). Single-cell analysis of tCycIF images focusing on PAX8- or CK7-positive cancer cells expressing pRPA32-RPA2(Ser8) revealed that, in line with previous findings, samples responsive to ATRi combinations exhibited higher levels of pRPA32-RPA2(Ser8) compared to non-responders (Figure 9). These results highlight the capability of our platform to facilitate screening for novel combination therapies in iPDCs, while also contributing to the exploration of tissue-based predictive biomarkers.

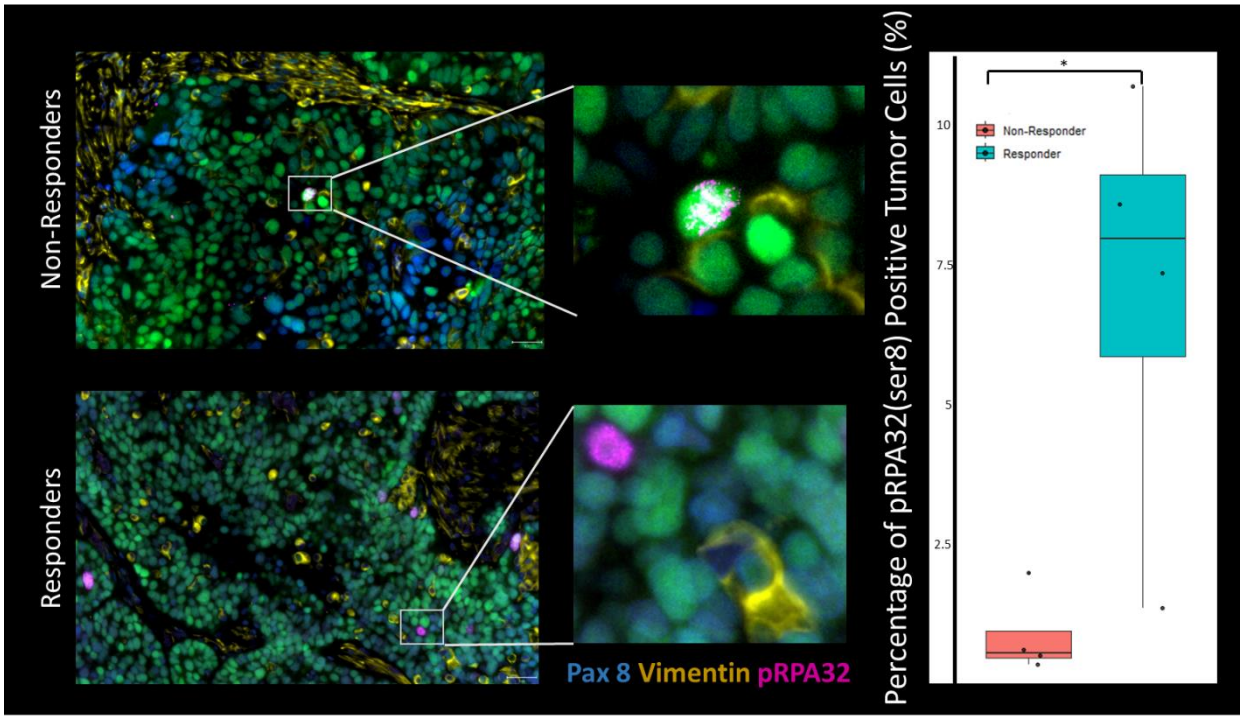

Figure 9. Significantly elevated replication stress marker, pRPA32, in tumor cells of responders compared to non-responders. Box-and-whisker plot of tumor cells expressing pRPA32-RPA2(Ser8) plotted as a percentage (right). Representative images from C105_A, non-responder, and C634, responder (left). Scale bar 150µm and 25µm. Mann-Whitney U-test $p^* < 0.05$.

4.3 Immune cell abundance, functional state, and spatial distribution in responders and non-responders

4.3.1 Consistent cell type abundance in TME across samples

The tumor microenvironment plays a critical role in tumorigenesis and is a promising target for HGSC treatment. To delineate the prevalent cell types, tCycIF analysis was conducted on corresponding FFPE tumor tissues obtained from the samples depicted in Figure 6. Using antibodies against PAX8 and CK7 (for tumor cells), vimentin (for stromal cells), and CD68, CD3D, CD4, CD8a, and CD11C (for immune cells), we assessed the relative abundance of tumor, stromal, and immune cells across the samples. Tumor cells were found to be the most abundant cell type in the majority of samples, followed by stromal cells, while immune cells comprised less than 20% of the total cell count across all samples (Figure 10).

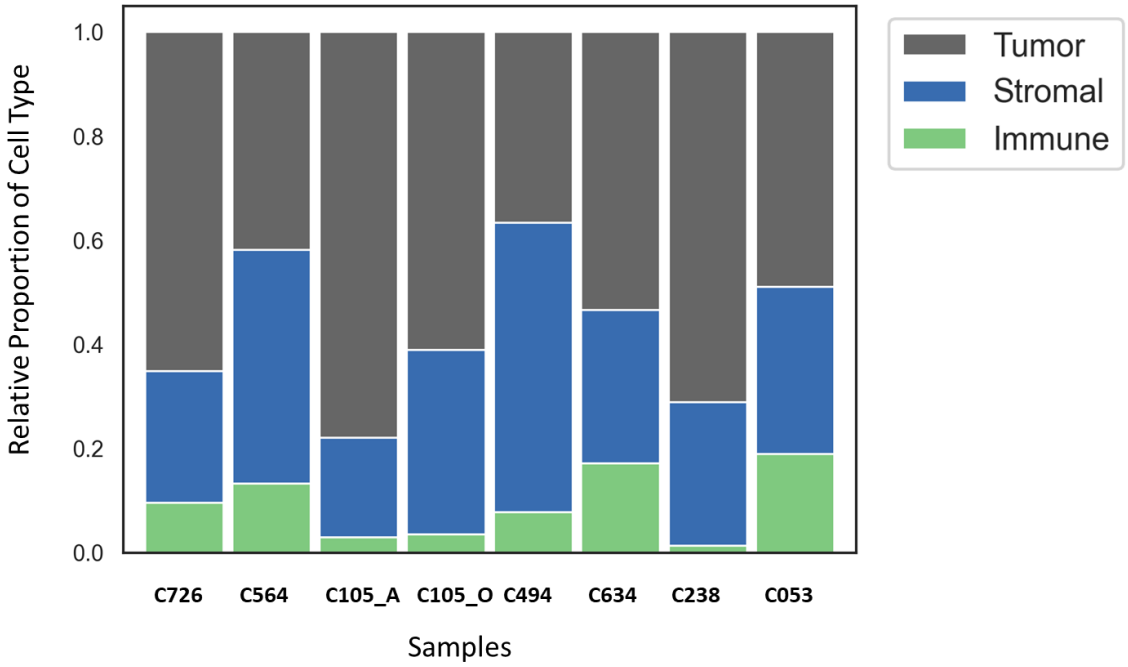

Figure 10. Consistent cell type abundance in TME across samples. The proportions are depicted in a stacked bar plot, summarizing relative proportion of tumor, stromal, and immune cells present per sample.

4.3.2 Myeloid cells represent the majority of immune cells within the TME

To further investigate patient-specific immune responses to ATRi monotherapy and in combination with other DNA damaging agents and immunotherapies noted in Figure

6, we used antibodies against CD68 and CD11C (for myeloid cells), CD3D (for T-cells), CD4 (for CD4+ T-cells) , CD8a (for CD8+ T-cells), and FoxP3 (for regulatory T-cells). Myeloid cells made up a majority of the immune cells present across all samples, comprising of macrophages (CD68+) and dendritic cells (CD11c+) (Figure 11). T-cells (CD8+ cells, CD4+ cells, and regulatory T-cells) were the next most prominent cell type.

Patient-specific variations were noted, as the presence of immune cell did not consistently correlate with the treatment response observed in the iPDCs. For example, despite relatively elevated CD8+ and CD4+ T-cells infiltration in sample C564, the CD45+ cells from this sample's iPDCs exhibited poor response to both DNA damaging agents and immunotherapies. Conversely, sample C726, which showed favorable response in the iPDCs, had relatively low T-cell populations. This suggests immune cell content in the TME alone may not fully predict anti-tumor immune activity.

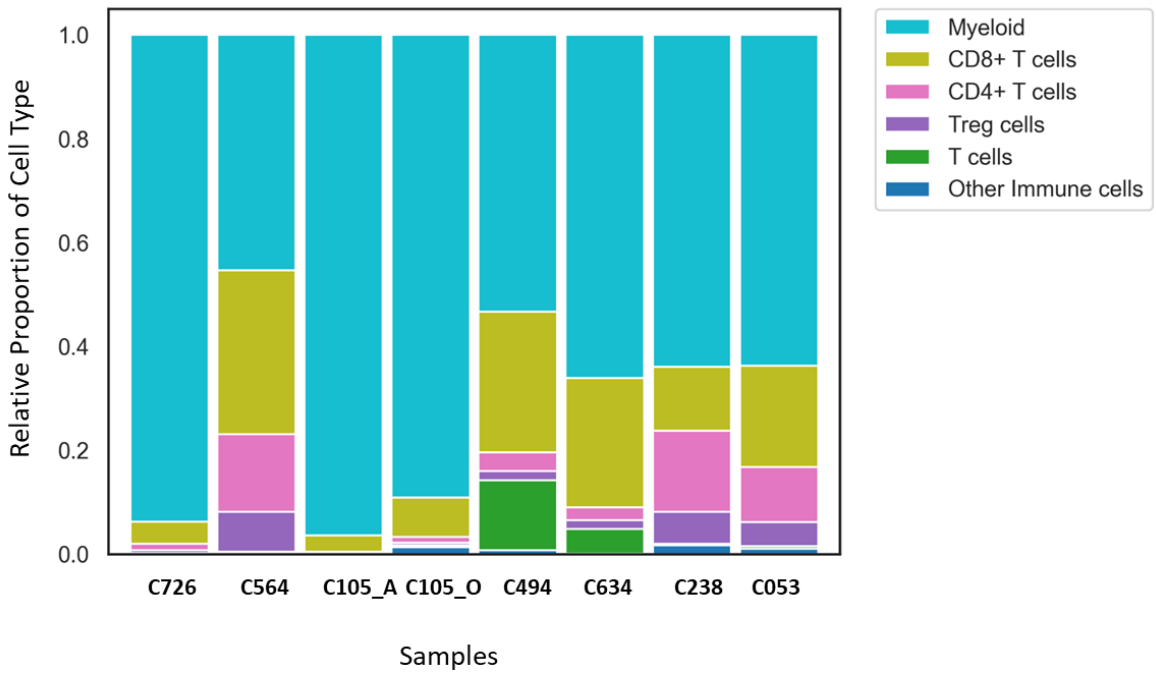

Figure 11. Myeloid cells represent the majority of immune cells in the TME.
The proportions are depicted in a stacked bar plot, summarizing the immune cell subtypes present per sample.

4.3.3 No significant discrepancy in functional T-cell activation in responders versus non-responders

To investigate potential differences in T-cell activation between groups, we utilized antibodies targeting CD3D (for T-cells), CD8a (for CD8+ T-cells), CD4 (for CD4+ T-cells), pSTAT1 (indicative of interferon signaling mediating anti-tumor immune response), granzyme B (associated with tumor immune surveillance), and PD-1 (a marker of T-cell exhaustion). Analysis of single-cell data from tCycIF images revealed no significant variation in the baseline functional immune states of CD8+ or CD4+ T-cells expressing markers such as granzyme B, PD-1, and pSTAT1 between responders and non-responders (Figure 12). While our expectation did not include immune activation predicting therapy response to DNA damaging agents, it's noteworthy that host immunity has been shown to significantly contribute to cancer prognosis (Zhang et al., 2003).

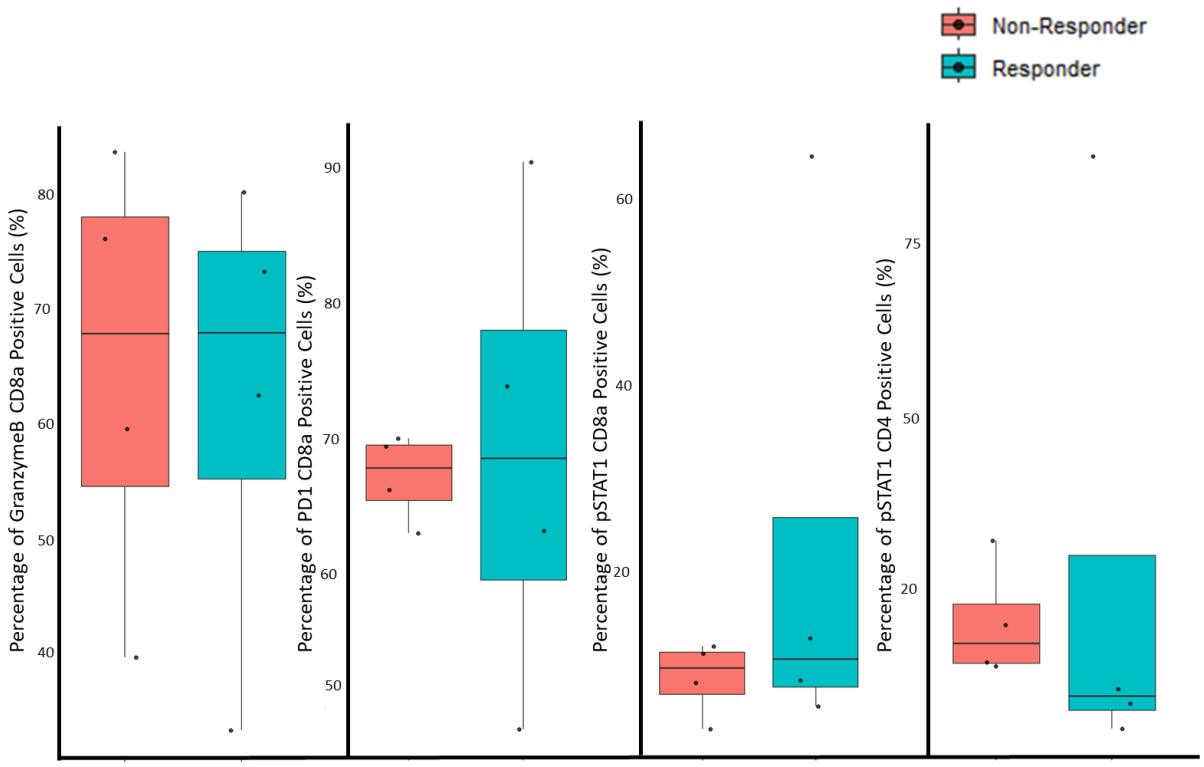

Figure 12. No significant discrepancy in functional CD8+ and CD4+ T-cell activation in responders versus non-responders. From left to right, box-and-whisker plots of CD8+ cells expressing granzyme B over all CD8+ cell per sample as a percentage, CD8+ cells expressing PD-1 over all CD8+ cell per sample as a percentage, CD8+ cells expressing pSTAT1 over all CD8+ cell per sample as a percentage, and CD4+ cells expressing pSTAT1 over all CD4+ cell per sample as a percentage.

4.3.4 Visually distinct intertumoral immune infiltration between responders and non-responders

Upon revisiting the multiplex tCycIF images of whole-slide tissue sections corresponding to patient samples cultured in the iPDCs, distinct spatial patterns emerged in CD4+ T-cells and activated CD8+ T-cells between responders and non-responders. While a comprehensive spatial analysis is warranted to quantify this observation, representative images from both groups revealed that CD4+ T-cells and CD8+ T-cells expressing granzyme B tended to infiltrate the tumor compartment in responders, whereas they congregated predominantly in the stromal region in non-responders (Figure 13). This finding aligns with the classification of hot tumors. It is plausible that the sensitivity observed in responders to ATRi monotherapy and its combination with DNA damaging agents and immunotherapies is driven by both genomic instability inherent in tumor cells and the infiltration of lymphocytes within the tumor compartment.

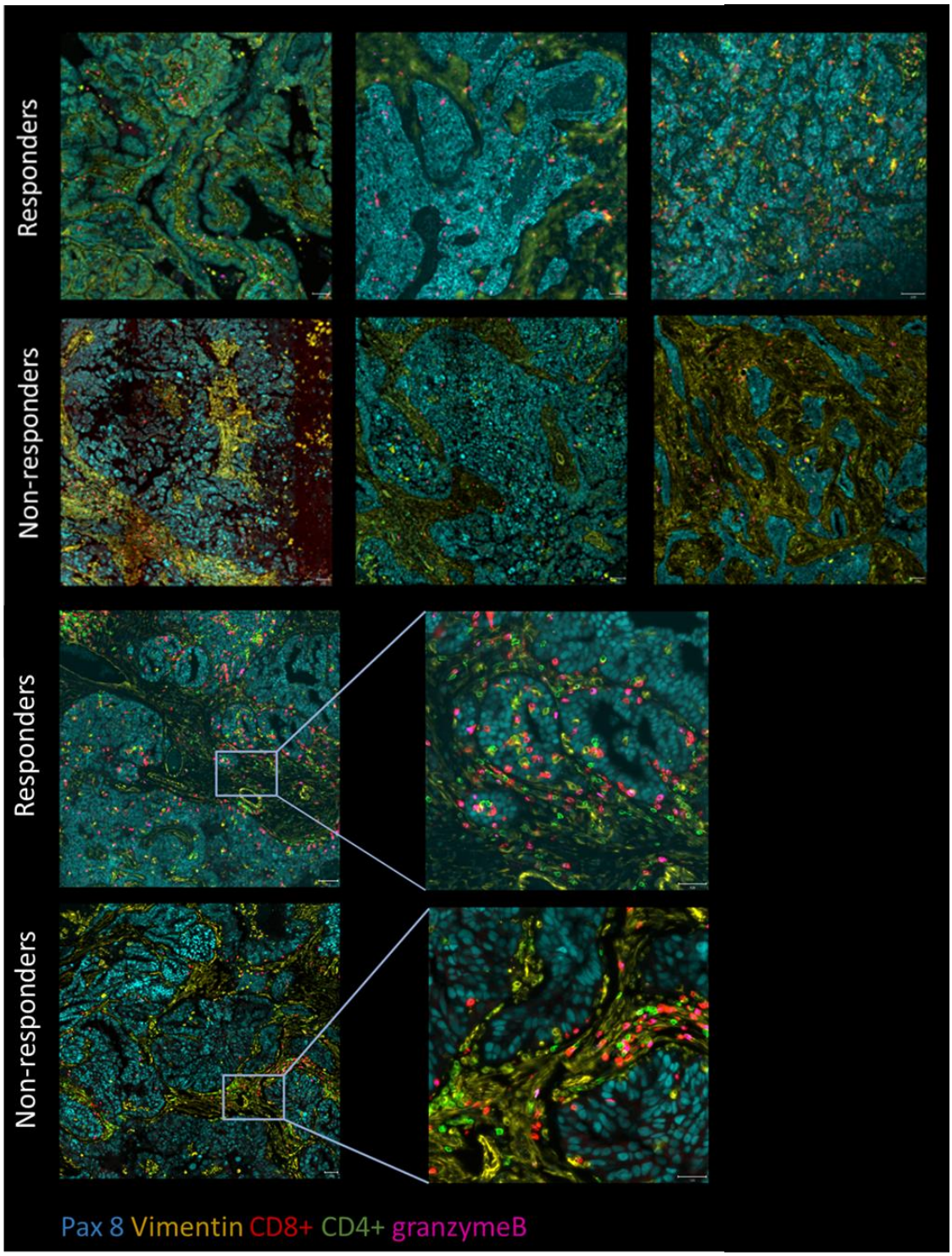

Figure 13. tCycIF images highlighting differential spatial patterns of activated T-cells in responders versus non-responders. Scale bar 200µm and 125µm.

5 Discussion

Preclinical models of HGSC have attempted to replicate the complexity within the tumor microenvironment to study cellular modifications, disease progression, and resistance to treatment. However, these models either do not faithfully recapitulate the tumor-promoting microenvironment or are not suitable for high-throughput drug screening (Mendoza-Martinez et al., 2021). Herein, the establishment of patient-derived immunocompetent cultures in a physiology comparable matrix by my colleagues and tissue-based biomarker investigation of corresponding samples provides a platform for functional testing of immuno-oncology agents tailored for precision oncology in HGSC.

Our lab developed a model of the tumor microenvironment in HGSC using patient-derived tumor samples while retaining intertumoral immune cells in culture. Preliminary results demonstrated improved cell growth using OmeGel, a patient-derived tumor-free omentum tissue matrix. Furthermore, clinical responses to chemotherapy and PARPi were replicated in our iPDCs. Next, high-throughput immune-oncology drug screening (n = 8) was performed on iPDCs, necessitating a method to consolidate the multi-dimensional output for analysis.

The development of an analysis and visualization pipeline allowed for drug response comparisons and highlighted patient-specific cytotoxic responses in tumor and immune cells. These observations are in line with treatment outcomes observed in the clinics, emphasizing tumor heterogeneity in HGSC (Roberts et al., 2019). Half of our samples responded to ATRi and its combinations, independent of HR status. To further delineate between responders and non-responders, multiplexed tissue-based biomarker investigation was employed to study the burden of DNA damage and replication stress in tumor cells and to characterize the immune cell abundance and functional states.

We report trends suggesting elevated DNA damage (increased γH2AX expression) in responders versus non-responders. While γH2AX expression correlates with decreased disease-free survival in patients (Mei et al., 2015), it may also serve as a therapeutic target. Furthermore, we found elevated expression of pCHK1 and significantly elevated expression of pRPA32-RPA2(Ser8) in Pax8- or CK7-positive tumor cells in responders, corroborating previous findings validating these markers as

biomarkers of ATRi sensitivity (Bradbury et al., 2022). The results would suggest that responder group samples are more dependent on replication stress pathways to address the accumulation of damaged DNA and therefore show greater sensitivity to ATRi. In addition to validating previous findings demonstrating the utility of pRPA32-RPA2(Ser8), we also validate the results in our iPDCs by demonstrating that samples that responded to DNA damaging agent ATRi in fact had elevated baseline DNA damage and upregulated replication stress pathway activity. Our findings are limited by sample size; however, the establishment of our platform will enable further data collection and analysis. We also note the non-canonical cytoplasmic staining pattern of nuclear marker pCHK1. This may be a technical issue requiring further validation of this marker, or warrants evaluating other antibodies targeting pCHK1. In addition, previous studies validated pCHK1 in high-grade cell lines, perhaps the discrepancies observed in this tissue-based investigation reflect biological relevancy not yet explored.

Using tCycIF, a multi-plex immunofluorescence technique, to characterize the TME we found that most samples consisted predominately of tumor cells. Among immune cells, myeloid cells were the most common immune cell type, consistent with previous results (Launonen et al., 2022). Given the relative abundance, heterogeneity of myeloid lineage cells, and demonstrated potential to drive pro-tumor activity, myeloid cells, particularly tumor-associated macrophages have been identified as targets to address poor response to immunotherapies (Truxova et al., 2023). However, in this study we chose to narrow our investigation and focused on infiltrating lymphocyte activation within the TME.

When examining the TME, we found no appreciable differences in the activation states of CD4+ and CD8+ T-cells. We examined granzyme B, associated with tumor immune surveillance, pSTAT1, indicative of interferon signaling mediating anti-tumor immune response, and PD-1, a marker of T-cell exhaustion. Previous work has found that baseline functional status of the TME, specifically increased STAT1 expression, served as a survival predictive biomarker in HGSC (Koti et al., 2015); however, we were unable to replicate this finding. Upon revisiting the multichannel raw images, we noticed distinct patterns in T-cell infiltration within the tumor compartment. Spatial neighborhood analyses performed on tCycIF data have shown distinct TME niches with increased immunosurveillance dependent on molecular subtype and increased tumor proliferation (Launonen et al., 2022). Therefore, further investigation

quantifying tumor immune cell interactions in our samples may provide additional pretext to the drug responses observed in the iPDCs.

In summary, we showcase the comprehensive utility of this integrated approach in evaluating potential combination therapies and validating treatment response through tissue-based biomarker investigations. By focusing on elucidating patient-specific differences within the TME that influence drug sensitivity, this research aims to deepen our understanding of the complex interplay between tumor biology and therapeutic response. Through this exploration, insights garnered could significantly contribute to optimizing treatment strategies tailored to individual patients, ultimately enhancing outcomes in oncology.

References

Armstrong, Deborah K., Ronald D. Alvarez, Jamie N. Bakkum-Gamez, Lisa Barroilhet, Kian Behbakht, Andrew Berchuck, Lee-may Chen, et al. “Ovarian Cancer, Version 2.2020, NCCN Clinical Practice Guidelines in Oncology.” *Journal of the National Comprehensive Cancer Network*, vol. 19, no. 2, Feb. 2021, pp. 191–226, https://doi.org/10.6004/jnccn.2021.0007.

Baker, Gregory J., et al. *Quality Control for Single Cell Analysis of High-Plex Tissue Profiles Using CyLinter*. 1 Nov. 2023, https://doi.org/10.1101/2023.11.01.565120.

Bogani, Giorgio, et al. “Immunotherapy for Platinum-Resistant Ovarian Cancer.” *Gynecologic Oncology*, vol. 158, no. 2, Aug. 2020, pp. 484–88, https://doi.org/10.1016/j.ygyno.2020.05.681.

Bowtell, David D., et al. “Rethinking Ovarian Cancer II: Reducing Mortality from High-Grade Serous Ovarian Cancer.” *Nature Reviews Cancer*, vol. 15, no. 11, 2015, pp. 668–79, https://doi.org/10.1038/nrc4019.

Bradbury, Alice, et al. “The Role of ATR Inhibitors in Ovarian Cancer: Investigating Predictive Biomarkers of Response.” *Cells*, vol. 11, no. 15, Aug. 2022, p. 2361, https://doi.org/10.3390/cells11152361.

“Cancer Statistics.” *Finnish Cancer Registry*, 3 July 2023, https://tilastot.syoparekisteri.fi/syovat.

Chae, Chang-Suk, et al. “Tumor-Derived Lysophosphatidic Acid Blunts Protective Type I Interferon Responses in Ovarian Cancer.” *Cancer Discovery*, vol. 12, no. 8, Aug. 2022, pp. 1904–21, https://doi.org/10.1158/2159-8290.CD-21-1181.

Chan, Angela My, et al. “Combined CCNE1 High-level Amplification and Overexpression Is Associated with Unfavourable Outcome in Tubo-ovarian High-grade Serous Carcinoma.” *The Journal of Pathology: Clinical Research*, vol. 6, no. 4, 2020, pp. 252–62, https://doi.org/10.1002/cjp2.168.

Curiel, Tyler J., et al. “Specific Recruitment of Regulatory T Cells in Ovarian Carcinoma Fosters Immune Privilege and Predicts Reduced Survival.” *Nature Medicine*, vol. 10, no. 9, 2004, pp. 942–49, https://doi.org/10.1038/nm1093.

DiSilvestro, Paul, et al. “Overall Survival With Maintenance Olaparib at a 7-Year Follow-Up in Patients With Newly Diagnosed Advanced Ovarian Cancer and a

BRCA Mutation: The SOLO1/GOG 3004 Trial." *Journal of Clinical Oncology*, vol. 41, no. 3, Jan. 2023, pp. 609–17, https://doi.org/10.1200/JCO.22.01549.

González-Martín, Antonio, et al. "Niraparib in Patients with Newly Diagnosed Advanced Ovarian Cancer." *New England Journal of Medicine*, vol. 381, no. 25, Dec. 2019, pp. 2391–402, https://doi.org/10.1056/NEJMoa1910962.

Hao, Jiatao, et al. "Prognostic Impact of Tumor-Infiltrating Lymphocytes in High Grade Serous Ovarian Cancer: A Systematic Review and Meta-Analysis." *Therapeutic Advances in Medical Oncology*, vol. 12, 2020, p. 175883592096724, https://doi.org/10.1177/1758835920967241.

Hensler, Michal, et al. "M2-like Macrophages Dictate Clinically Relevant Immunosuppression in Metastatic Ovarian Cancer." *Journal for ImmunoTherapy of Cancer*, vol. 8, no. 2, 2020, p. e000979, https://doi.org/10.1136/jitc-2020-000979.

Kloosterman, Daan J., and Leila Akkari. "Macrophages at the Interface of the Co-Evolving Cancer Ecosystem." *Cell*, vol. 186, no. 8, 2023, pp. 1627–51, https://doi.org/10.1016/j.cell.2023.02.020.

Konstantinopoulos, Panagiotis A., et al. "Single-Arm Phases 1 and 2 Trial of Niraparib in Combination With Pembrolizumab in Patients With Recurrent Platinum-Resistant Ovarian Carcinoma." *JAMA Oncology*, vol. 5, no. 8, Aug. 2019, pp. 1141–49, https://doi.org/10.1001/jamaoncol.2019.1048.

Koti, M., et al. "A Distinct Pre-Existing Inflammatory Tumour Microenvironment Is Associated with Chemotherapy Resistance in High-Grade Serous Epithelial Ovarian Cancer." *British Journal of Cancer*, vol. 112, no. 7, Mar. 2015, pp. 1215–22, https://doi.org/10.1038/bjc.2015.81.

Larionova, Irina, et al. "Tumor-Associated Macrophages in Human Breast, Colorectal, Lung, Ovarian and Prostate Cancers." *Frontiers in Oncology*, vol. 10, Oct. 2020, p. 566511, https://doi.org/10.3389/fonc.2020.566511.

Launonen, I. M., et al. "Single-Cell Tumor-Immune Microenvironment of BRCA1/2 Mutated High-Grade Serous Ovarian Cancer." *Nature Communications*, vol. 13, no. 1, Feb. 2022, p. 835, https://doi.org/10.1038/s41467-022-28389-3.

Lecker, Laura S. M., et al. "TGFBI Production by Macrophages Contributes to an Immunosuppressive Microenvironment in Ovarian Cancer." *Cancer Research*, vol. 81, no. 22, Nov. 2021, pp. 5706–19, https://doi.org/10.1158/0008-5472.CAN-21-0536.

Ledermann, Jonathan, et al. “Olaparib Maintenance Therapy in Platinum-Sensitive Relapsed Ovarian Cancer.” *New England Journal of Medicine*, vol. 366, no. 15, Apr. 2012, pp. 1382–92, https://doi.org/10.1056/NEJMoa1105535.

Lheureux, Stephanie, Mihaela C. Cristea, et al. “Adavosertib plus Gemcitabine for Platinum-Resistant or Platinum-Refractory Recurrent Ovarian Cancer: A Double-Blind, Randomised, Placebo-Controlled, Phase 2 Trial.” *Lancet (London, England)*, vol. 397, no. 10271, Jan. 2021, pp. 281–92, https://doi.org/10.1016/S0140-6736(20)32554-X.

Lheureux, Stephanie, Ana Oaknin, et al. “EVOLVE: A Multicenter Open-Label Single-Arm Clinical and Translational Phase II Trial of Cediranib Plus Olaparib for Ovarian Cancer after PARP Inhibition Progression.” *Clinical Cancer Research*, vol. 26, no. 16, Aug. 2020, pp. 4206–15, https://doi.org/10.1158/1078-0432.CCR-19-4121.

Li, Siyu, et al. “ATR Inhibitors in Platinum-Resistant Ovarian Cancer.” *Cancers*, vol. 14, no. 23, Nov. 2022, p. 5902, https://doi.org/10.3390/cancers14235902.

Li, Xuan, and Wolf-Dietrich Heyer. “Homologous Recombination in DNA Repair and DNA Damage Tolerance.” *Cell Research*, vol. 18, no. 1, Jan. 2008, pp. 99–113, https://doi.org/10.1038/cr.2008.1.

Lin, Jia-Ren, et al. “Highly Multiplexed Immunofluorescence Imaging of Human Tissues and Tumors Using T-CyCIF and Conventional Optical Microscopes.” *ELife*, vol. 7, July 2018, p. e31657, https://doi.org/10.7554/eLife.31657.

Lisio, Michael-Antony, et al. “High-Grade Serous Ovarian Cancer: Basic Sciences, Clinical and Therapeutic Standpoints.” *International Journal of Molecular Sciences*, vol. 20, no. 4, Feb. 2019, p. 952, https://doi.org/10.3390/ijms20040952.

Matulonis, Ursula A., et al. “Ovarian Cancer.” *Nature Reviews Disease Primers*, vol. 2, no. 1, Aug. 2016, p. 16061, https://doi.org/10.1038/nrdp.2016.61.

Mei, Ling, et al. “Phospho-Histone H2AX Is a Diagnostic and Prognostic Marker for Epithelial Ovarian Cancer.” *International Journal of Clinical and Experimental Pathology*, vol. 8, no. 5, 2015, pp. 5597–602.

Mendoza-Martinez, Ana Karen, et al. “Modeling the Tumor Microenvironment of Ovarian Cancer: The Application of Self-Assembling Biomaterials.” *Cancers*, vol. 13, no. 22, Nov. 2021, p. 5745, https://doi.org/10.3390/cancers13225745.

Mikuła-Pietrasik, Justyna, et al. “Comprehensive Review on How Platinum- and Taxane-Based Chemotherapy of Ovarian Cancer Affects Biology of Normal Cells.” *Cellular and Molecular Life Sciences*, vol. 76, no. 4, 2019, pp. 681–97, https://doi.org/10.1007/s00018-018-2954-1.

Mohamed, Eslam, et al. “The Unfolded Protein Response Mediator PERK Governs Myeloid Cell-Driven Immunosuppression in Tumors through Inhibition of STING Signaling.” *Immunity*, vol. 52, no. 4, 2020, pp. 668-682.e7, https://doi.org/10.1016/j.immuni.2020.03.004.

Momenimovahed, Zohre, et al. “Ovarian Cancer in the World: Epidemiology and Risk Factors.” *International Journal of Women’s Health*, vol. 11, Apr. 2019, pp. 287–99, https://doi.org/10.2147/IJWH.S197604.

Moore, Kathleen, et al. “Maintenance Olaparib in Patients with Newly Diagnosed Advanced Ovarian Cancer.” *New England Journal of Medicine*, vol. 379, no. 26, Dec. 2018, pp. 2495–505, https://doi.org/10.1056/NEJMoa1810858.

Moore, Kathleen N., et al. “Atezolizumab, Bevacizumab, and Chemotherapy for Newly Diagnosed Stage III or IV Ovarian Cancer: Placebo-Controlled Randomized Phase III Trial (IMagyn050/GOG 3015/ENGOT-OV39).” *Journal of Clinical Oncology*, vol. 39, no. 17, June 2021, pp. 1842–55, https://doi.org/10.1200/JCO.21.00306.

Muhlich, Jeremy L., et al. “Stitching and Registering Highly Multiplexed Whole-Slide Images of Tissues and Tumors Using ASHLAR.” *Bioinformatics*, edited by Alfonso Valencia,vol. 38, no. 19, Sept. 2022, pp. 4613–21, https://doi.org/10.1093/bioinformatics/btac544.

Nagaraj, Ashwini S., et al. *Patient-Derived Functional Immuno-Oncology Platform Identifies Responders to ATR Inhibitor and Immunotherapy Combinations in Ovarian Cancer*. 19 Feb. 2024, https://doi.org/10.1101/2024.02.15.579904.

Neal, James T., et al. “Organoid Modeling of the Tumor Immune Microenvironment.” *Cell*, vol. 175, no. 7, Dec. 2018, pp. 1972-1988.e16, https://doi.org/10.1016/j.cell.2018.11.021.

Neilson, Lisa J., et al. “Omentum-Derived Matrix Enables the Study of Metastatic Ovarian Cancer and Stromal Cell Functions in a Physiologically Relevant Environment.” *Matrix Biology Plus*, vol. 19–20, Dec. 2023, p. 100136, https://doi.org/10.1016/j.mbplus.2023.100136.

Nieman, Kristin M., et al. “Adipocytes Promote Ovarian Cancer Metastasis and Provide Energy for Rapid Tumor Growth.” *Nature Medicine*, vol. 17, no. 11, Nov. 2011, pp. 1498–503, https://doi.org/10.1038/nm.2492.

Ning, Franklin, et al. “Driving Immune Responses in the Ovarian Tumor Microenvironment.” *Frontiers in Oncology*, vol. 10, Jan. 2021, https://doi.org/10.3389/fonc.2020.604084.

Oza, Amit M., et al. “Standard Chemotherapy with or without Bevacizumab for Women with Newly Diagnosed Ovarian Cancer (ICON7): Overall Survival Results of a Phase 3 Randomised Trial.” *The Lancet Oncology*, vol. 16, no. 8, 2015, pp. 928–36, https://doi.org/10.1016/S1470-2045(15)00086-8.

Palla, Viktoria-Varvara, et al. “Gamma-H2AX: Can It Be Established as a Classical Cancer Prognostic Factor?” *Tumor Biology*, vol. 39, no. 3, 2017, p. 101042831769593, https://doi.org/10.1177/1010428317695931.

Perez-Villatoro, Fernando, et al. “Optimized Detection of Homologous Recombination Deficiency Improves the Prediction of Clinical Outcomes in Cancer.” *Npj Precision Oncology*, vol. 6, no. 1, Dec. 2022, pp. 1–13, https://doi.org/10.1038/s41698-022-00339-8.

Rabik, Cara A., and M. Eileen Dolan. “Molecular Mechanisms of Resistance and Toxicity Associated with Platinating Agents.” *Cancer Treatment Reviews*, vol. 33, no. 1, 2007, pp. 9–23, https://doi.org/10.1016/j.ctrv.2006.09.006.

Ray-Coquard, Isabelle, et al. “Olaparib plus Bevacizumab as First-Line Maintenance in Ovarian Cancer.” *New England Journal of Medicine*, vol. 381, no. 25, Dec. 2019, pp. 2416–28, https://doi.org/10.1056/NEJMoa1911361.

Robert, Caroline. “A Decade of Immune-Checkpoint Inhibitors in Cancer Therapy.” *Nature Communications*, vol. 11, no. 1, July 2020, p. 3801, https://doi.org/10.1038/s41467-020-17670-y.

Roberts, Cai M., et al. “The Role of Intra-Tumoral Heterogeneity and Its Clinical Relevance in Epithelial Ovarian Cancer Recurrence and Metastasis.” *Cancers*, vol. 11, no. 8, July 2019, p. 1083, https://doi.org/10.3390/cancers11081083.

Rose, Maddison, et al. “PARP Inhibitors: Clinical Relevance, Mechanisms of Action and Tumor Resistance.” *Frontiers in Cell and Developmental Biology*, vol. 8, Sept. 2020, p. 564601, https://doi.org/10.3389/fcell.2020.564601.

Schapiro, Denis, et al. “MCMICRO: A Scalable, Modular Image-Processing Pipeline for Multiplexed Tissue Imaging.” *Nature Methods*, vol. 19, no. 3, Mar. 2022, pp. 311–15, https://doi.org/10.1038/s41592-021-01308-y.

Schmidt, Uwe, et al. “Cell Detection with Star-Convex Polygons.” *Medical Image Computing and Computer Assisted Intervention – MICCAI 2018*, edited by Alejandro F. Frangi et al., vol. 11071, Springer International Publishing, 2018, pp. 265–73, https://doi.org/10.1007/978-3-030-00934-2_30.

Siegel, Rebecca L., et al. “Cancer Statistics, 2023.” *CA: A Cancer Journal for Clinicians*, vol. 73, no. 1, 2023, pp. 17–48, https://doi.org/10.3322/caac.21763.

Sofroniew, Nicholas, et al. *Napari: A Multi-Dimensional Image Viewer for Python*. v0.4.16, Zenodo, 2022, https://doi.org/10.5281/ZENODO.6598542.

The Cancer Genome Atlas Research Network. “Integrated Genomic Analyses of Ovarian Carcinoma.” *Nature*, vol. 474, no. 7353, June 2011, pp. 609–15, https://doi.org/10.1038/nature10166.

Truxova, Iva, et al. “Targeting Tumor-Associated Macrophages for Successful Immunotherapy of Ovarian Carcinoma.” *Journal for ImmunoTherapy of Cancer*, vol. 11, no. 2, Feb. 2023, p. e005968, https://doi.org/10.1136/jitc-2022-005968.

Voabil, Paula, et al. “An Ex Vivo Tumor Fragment Platform to Dissect Response to PD-1 Blockade in Cancer.” *Nature Medicine*, vol. 27, no. 7, 2021, pp. 1250–61, https://doi.org/10.1038/s41591-021-01398-3.

Wan, Changxin, et al. “Enhanced Efficacy of Simultaneous PD-1 and PD-L1 Immune Checkpoint Blockade in High-Grade Serous Ovarian Cancer.” *Cancer Research*, vol. 81, no. 1, Jan. 2021, pp. 158–73, https://doi.org/10.1158/0008-5472.CAN-20-1674.

Zhang, Lin, et al. “Intratumoral T Cells, Recurrence, and Survival in Epithelial Ovarian Cancer.” *New England Journal of Medicine*, vol. 348, no. 3, Jan. 2003, pp. 203–13, https://doi.org/10.1056/NEJMoa020177.